Supporting Information for "Anticyclones drive Beaufort breakout events"

MacKenzie E. Jewell[1], Jennifer K. Hutchings[1]

[1]College of Earth, Ocean, and Atmospheric Sciences, Oregon State University, 104 CEOAS Administration Building, Corvallis, OR 97331, USA

Contents of this file

1. Texts S1 to S2
2. Figures S1 to S4
3. Tables S1 to S2

Additional Supporting Information (Files uploaded separately)

1. Caption for Movie S1

Text S1. Typical breakout event sequence: While breakouts can be driven by a range of anticyclonic forcing conditions, the typical sequence begins with a high pressure system residing north or west of the Alaskan coast. Northeasterly winds produce wide leads that extend northward offshore from Point Barrow, the headland that divides the Beaufort and Chukchi Seas. These leads include small scale arched patterns such as Beaufort Arches (BA) (Figure 1a), wider arches called Wide Beaufort Arches (WBA), or

larger arched leads called Tangent Arc (TA) leads (Figure 1b-d) that extend hundreds of kilometers offshore tangent to the Chukchi coast (Lewis & Hutchings, 2019). If the anticyclone progresses eastward, wind direction over the Beaufort Sea shifts westward and additional leads open stepwise eastward along the Alaskan coast. Such leads include Wide Angle (WA) leads (Figure 1f) and High Angle (HA) leads (Figure 1g) which extend northward offshore from the central and eastern coast of Alaska, respectively. Once the anticyclone has traveled eastward over land, or its orientation has changed to sufficiently increase the alongshore-component of wind forcing over the Beaufort Sea, an East Coastal (EC) flaw lead (Figure 1e-h) opens parallel to Banks Island at the eastern boundary of the Beaufort Sea. The opening of this lead indicates the transition to a breakout event in which the entire ice pack breaks away from its coastal boundaries and accelerates. When EC leads are present, ice flux along the Alaskan coast is double its average magnitude (Lewis & Hutchings, 2019). As a breakout event continues, extensive fracturing and ice acceleration extend across the Beaufort Sea until the anticyclone exits the region or its orientation changes to reduce along-shore wind forcing.

Text S2.

Comparison of simulation to observations: Depending on the forcing used, neXtSIM captured the progression across all or some of the BA, TA, WA, HA, and EC lead patterns that occurred during the 2013 event (Figures S2 and S3). The occurrence of these coastal lead patterns is sensitive to the pattern of wind forcing near the coast. Given this sensitivity, the variability in the timing and progression of simulated lead patterns across simulations with different forcing models is to be expected. Across simulations,

neXtSIM consistently captured the expected structure of coastal lead patterns, including primary and secondary fractures of TA and WA leads, the ice motion along the fractures, and their termination in the center of the passing anticyclone. See in the ERA5 31-km and polarWRF 10-km simulations, for example, features resembling BA leads (Figures S3b and S2b-d) and TA leads (Figures S3c and S2d) that extend from Point Barrow, WA leads (Figure S2d) that extend from the central coast of Alaska, and EC leads (Figures S3d-h and S2e-h) along the eastern coast of the Beaufort Sea.

Differences between observed and simulated leads early in the event also speak to the strength of the model (Figures S3b and S2b). On February 16, a broad arched lead formed through a region of previously heavily deformed ice, reactivating a dormant TA lead that originally opened on February 10 (see Supplementary Movie S1). As this activity occurred before the simulation began on February 13, the observed impacts of these anisotropic features on subsequent ice dynamics was not present in the model, and none of the simulations captured this lead pattern.

Under a range of forcing conditions and initial ice thicknesses, neXtSIM also consistently represented the delineation of ice drift regimes along leads (Figures S1a,c,d, S2, and S3). As observed (Figure S1e), the ice pack was stationary upwind of the leads but accelerated immediately downwind where the ice lost contact with the coast. This structure was not captured in the mEVP and EVP simulations, which exhibited more smoothly-varying fields (Figure S1b).

The primary difference between the neXtSIM simulations and observations was an underestimation of ice drift speed downwind of the leads. The ratio of ice drift to wind speed

was consistently underestimated (Figure S1), even when forced with different atmospheric models across which the wind speed varied by ± 4 m/s.

Movie S1.

Three-daily animation of 2013 Beaufort breakout event from February 5 to March 20. Thermal infrared MODIS imagery (Band 31) from NASA/Terra (MODIS Characterization Support Team (MCST), 2017) shows sea ice (light shades) and open water or thin ice (dark shades). Land mask overlain in grey. Hourly ten meter winds (purple arrows) and sea level pressure (colored contours, hPa) from ERA5 reanalysis (Hersbach et al., 2018) overlain for nearest hour preceding each image. Daily sea ice drift from NSIDC Polar Pathfinder (Tschudi et al., 2019) overlain as black arrows.

References

Hersbach, H., Bell, B., Berrisford, P., Biavati, G., Horányi, A., Muñoz Sabater, J., ... Thépaut, J.-N. (2018). *Era5 hourly data on single levels from 1959 to present* [dataset]. Copernicus Climate Change Service (C3S) Climate Data Store (CDS). Retrieved from `https://doi.org/10.24381/cds.adbb2d47` (Accessed: 2022-06-22) doi: 10.24381/cds.adbb2d47

Lewis, B. J., & Hutchings, J. K. (2019). Leads and associated sea ice drift in the Beaufort Sea in winter. *Journal of Geophysical Research: Oceans*, *124*, 3411–3427. doi: 10.1029/2018JC014898

MODIS Characterization Support Team (MCST). (2017). *Modis 1km calibrated radiances product* [dataset]. NASA MODIS Adaptive Processing System, Goddard Space Flight Center, USA. Retrieved from `http://dx.doi.org/10.5067/MODIS/MOD021KM.061`

(Accessed: 2022-06-22) doi: 10.5067/MODIS/MOD021KM.061

Rheinlænder, J. W., Davy, R., Ólason, E., Rampal, P., Spensberger, C., Williams, T. D., ... Spengler, T. (2022). Driving mechanisms of an extreme winter sea ice breakup event in the Beaufort Sea. *Geophysical Research Letters*, *49*(e2022GL099024). doi: 10.1029/2022GL099024

Tschudi, M., Meier, W. N., Stewart, J. S., Fowler, C., & Maslanik, J. (2019). *Polar pathfinder daily 25 km ease-grid sea ice motion vectors, version 4* [dataset]. Boulder, Colorado USA. NASA National Snow and Ice Data Center Distributed Active Archive Center. Retrieved from `https://doi.org/10.5067/INAWUWO7QH7B` (Accessed: 2022-06-22) doi: 10.5067/INAWUWO7QH7B

Willmes, S., & Heinemann, G. (2015). *Daily pan-arctic sea-ice lead maps for 2003-2015, with links to maps in netcdf format* [dataset]. PANGAEA. Retrieved from `https://doi.org/10.1594/PANGAEA.854411` (Accessed: 2022-06-22) doi: 10.1594/PANGAEA.854411

Table S1. Dates (month/day) of $\Delta P(70°N, 80°N) > 20\,hPa$ along $145°W$ from January-April 1979-2022 from ERA5 (Hersbach et al., 2018). Only sequences of 4 days or longer (one standard deviation above the mean duration of 2 days) displayed. Sequences 7 days or longer (3 standard deviations above the mean) are bold.

Year	Dates	Year	Dates
1979		2001	2/25-28, 3/2-5
1980	1/18-22	2002	2/28-3/3
1981	2/27-3/3, 3/15-20	2003	
1982		2004	
1983	**1/31-2/8**, 4/18-22	2005	
1984		2006	
1985	1/17-20	2007	
1986	1/5-10, 4/14-17	2008	2/12-15
1987	2/19-24, 3/20-24	2009	
1988		2010	2/11-16, 3/27-30
1989		2011	1/3-6
1990		2012	
1991		2013	**2/21-3/2**, 3/6-9
1992	1/8-11, 3/8-11, 4/16-19	2014	3/15-18
1993	2/26-3/1	2015	
1994		2016	1/25-28, 2/11-15, **2/25-3/2**, **4/6-12**, 4/21-24
1995	4/2-6	2017	
1996	4/5-8	2018	3/8-12
1997		2019	
1998	1/24-28, 2/19-22	2020	
1999		2021	1/8-13
2000	4/19-22	2022	

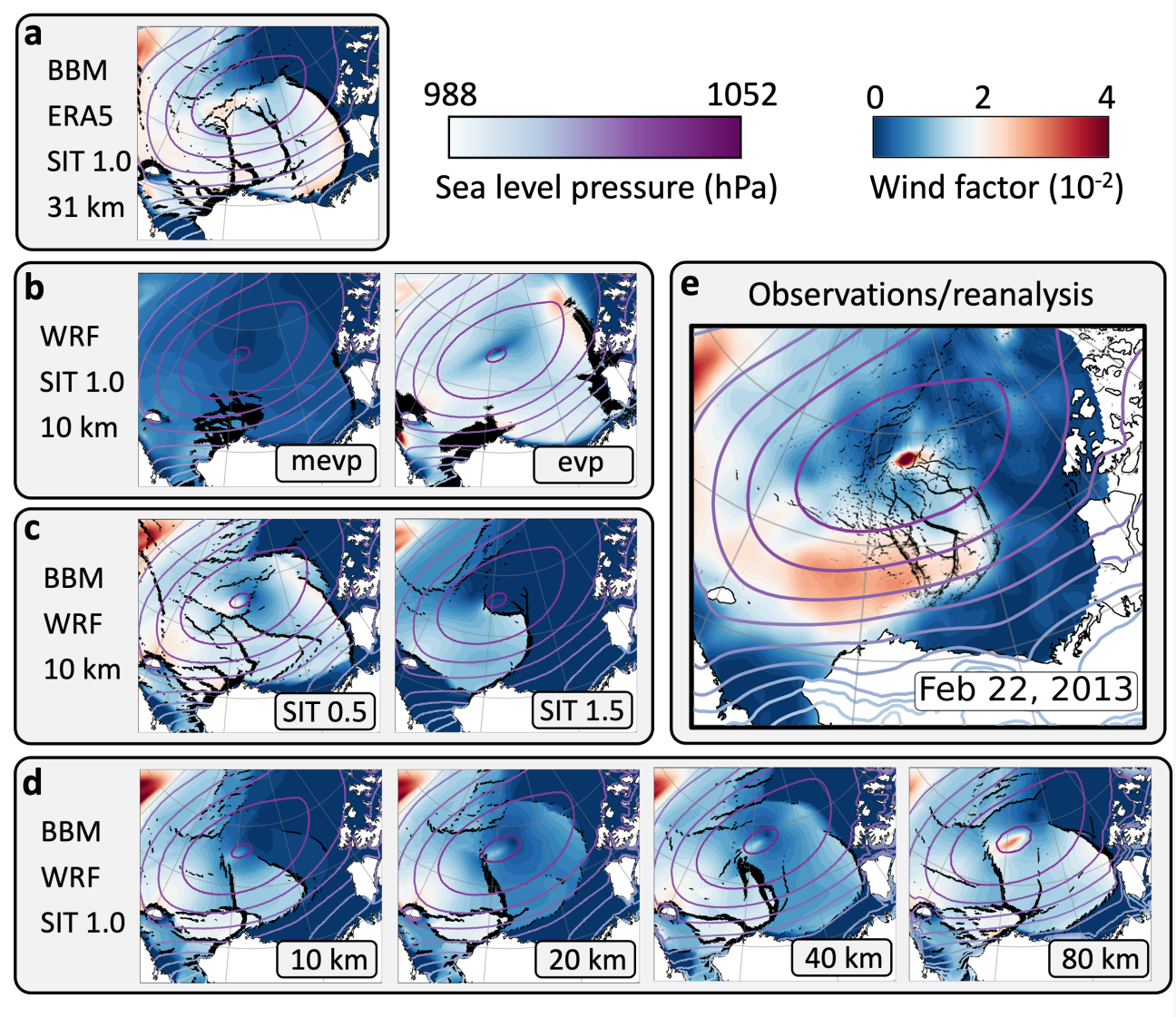

Figure S1. Daily wind factor (ratio of ice drift to wind speed) on Feb 22, 2013 for different neXtSIM simulation runs (a-d) (Rheinlænder et al., 2022). Regions filled with greater than 1% open water or thin sea ice shown in black. Contours are sea level pressure from forcing product. Rheology (BBM, evp, mevp), forcing product (ERA5, polarWRF), forcing resolution (10 – 80 km), and initial sea ice thickness (SIT 0.5 – 1.5) labeled for each set of simulations. Runs with no dynamics and with SIT 2.0 not shown as both show little activity at this time. Panel (e) shows wind factor from daily ERA5 reanalysis (Hersbach et al., 2018) and NSIDC Polar Pathfinder sea ice drift (Tschudi et al., 2019). Observed leads from Willmes and Heinemann (2015) shown in black. Note that clouds obscure leads near the coast.

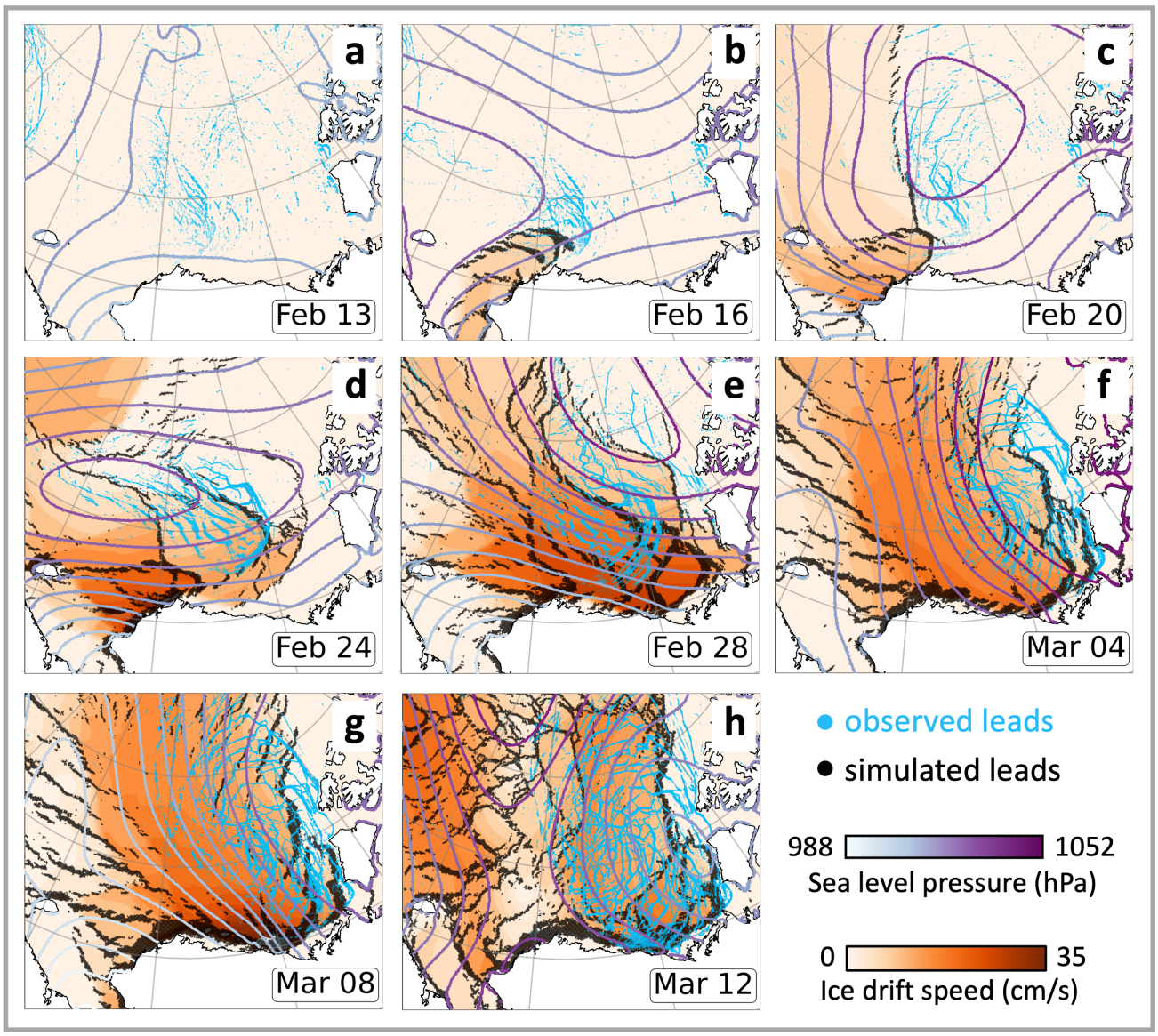

Figure S2. Daily average conditions from polarWRF 10 km resolution run. Color scale indicates ice drift speed. Regions filled with greater than 1% open water or thin sea ice shown in black. Contours are sea level pressure from forcing product. Observed leads from Willmes and Heinemann (2015) overlain in blue. Note that clouds sometimes obscure leads, particularly near the coast and in the west. Panels match dates of Figure 1, except the first panel starts on initial simulation date 2/13.

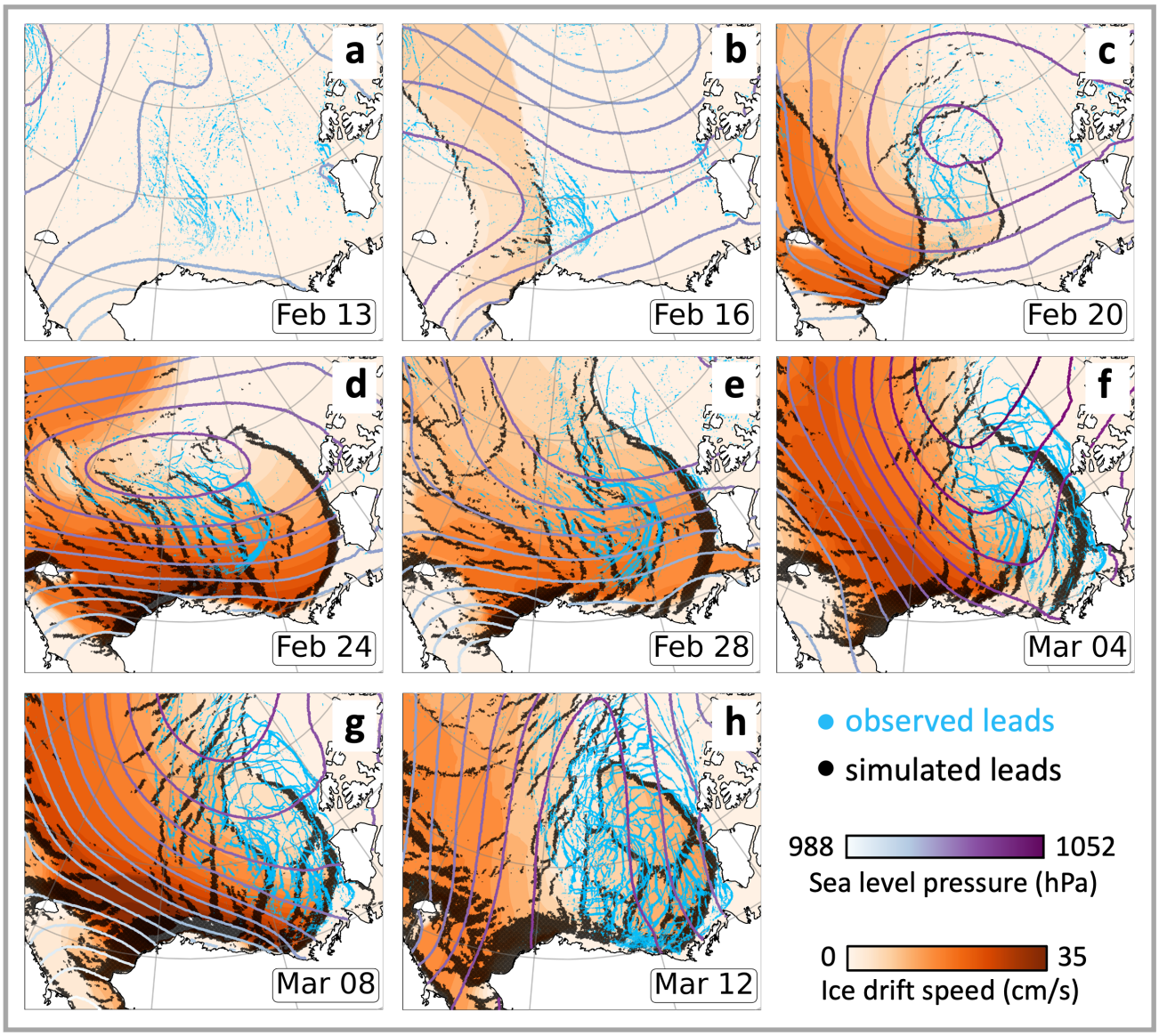

Figure S3. Same as Figure S2 but for the simulation forced with ERA5 (31 km).

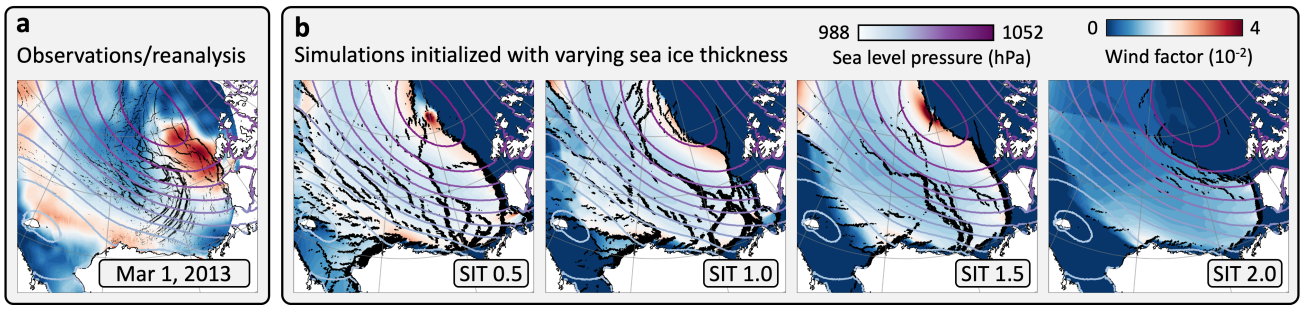

Figure S4. (a) Observed daily wind factor (ratio of ice drift to wind speed) on Mar 1, 2013 comparing polarWRF 10 km wind forcing to NSIDC observationally-derived drift speed (Tschudi et al., 2019). Observed leads from Willmes and Heinemann (2015) are overlain in black. Contours are sea level pressure from forcing product. (b) Mar 1, 2013 wind factor for different neXtSIM simulations forced with the same polarWRF 10 km model but initialized with different ice thicknesses relative to the observed thickness used in the primary simulation (SIT 1.0). Regions filled with greater than 1% open water or thin sea ice shown in black.

Table S2. Dates (month/day) of lead pattern sequences from Jan-Apr 1993-2013 identified by Lewis and Hutchings (2019). Only sequences of length greater or equal to mean duration displayed. Bold dates are sequences of length greater or equal to the duration of 2013 event patterns.

Year	EC	WA	TA
1993			
1994	1/1-10, 4/5-17		
1995	4/5-13		
1996	4/5-9	**4/9-10**	
1997			
1998	1/25-28		**1/15-24**
1999			
2000		**4/11-12**	2/12-15, 2/19-21
2001	1/9-15	**3/20-22**, **4/7-8**	
2002	2/5-9, 2/27-3/3		2/16-19
2003	1/11-15, 1/17-21, 3/1-3/5, 4/16-28	**4/11-12**	
2004		**1/25-27**	**1/20-24**
2005	2/14-18, 4/13-16	**3/22-24**	**4/10-16**
2006	4/3-6	**3/14-15**	
2007	1/15-20, 2/14-18	**4/18-19**	
2008	4/5-12	**3/30-31**	
2009	2/7-12, 3/14-17, **4/11-26**	**1/1-2**, **4/1-7**	
2010		**3/20-21**, **3/23-24**	
2011		**2/16-19**,**3/1-2**,**3/4-5**	**4/9-11**
2012			**4/8-13**
2013	**2/28-3/13**, 3/20-26	**3/4-5**	**1/30-2/4**, **2/20-24**
mean duration	4	2	3